24-093

Validation of Modeled Rockmass Permeability Against Field Measurements in a Longwall Mine

Zoheir Khademian
CDC NIOSH, Pittsburgh Mining Research Division, Pittsburgh, PA

Steven J. Schatzel
CDC NIOSH, Pittsburgh Mining Research Division, Pittsburgh, PA

Marcia M. Harris
CDC NIOSH, Pittsburgh Mining Research Division, Pittsburgh, PA

Kayode M. Ajayi
CDC NIOSH, Pittsburgh Mining Research Division, Pittsburgh, PA

ABSTRACT

Predicting rockmass permeability is critical in evaluating various engineering designs, including estimating gas inflow to a longwall mine in the case of a hypothetical breach in the gas well. This study conducted field permeability measurements to validate a geomechanical model capable of predicting rockmass permeability during longwall mining. A series of slug permeability tests were conducted in an active mine in Pennsylvania. A model of the mine was constructed in 3DEC numerical modeling software, and permeabilities were calculated. The modeling results agreed well with the pre- and post-mining permeability measurements, showing the applicability of this tool to evaluate gas well stability near mine workings.

INTRODUCTION

The intrinsic permeability of a rock or soil is a measure of the rock or soil's ability to transmit fluid as the fluid moves through it (Schwartz and Zhang, 2003). Evaluation of rockmass permeability is essential in various rock engineering designs such as constructing dams (Thawatchai, Bunpoat, & Warakorn, 2021), tunnels (K. Zhang et al., 2021), geothermal reservoirs (Tomac & Sauter, 2018), oil and gas reservoirs (Gehne & Benson, 2019), and waste containment structures (Sasaki & Rutqvist, 2021). Another application is the evaluation of permeabilities enhanced by mining where shale gas reservoirs underlie active or future longwall mining operations (PADEP, 2018). In the Northern Appalachian Basin in the United States, some of the production wells in shale gas reservoirs intersect with minable coal seams and thus require specific design considerations to allow both operations to coexist. In most cases, the gas wells are positioned in the mine abutment pillars for protection against mining-induced ground deformations. However, one of the safety concerns is excessive ground movement that might damage gas well production casing, leading to the leakage of explosive gas into the mine working. Under such scenario, mining-induced rockmass permeabilities and relevant changes induced by mining becomes of main importance.

In previous work (Khademian, et al. 2021)(Khademian, et al. 2021), a geomechanical modeling methodology was developed based on the Discrete Fracture Network (DFN) technique to calculate the permeability evolution during mining of a shallow, 145-m-cover mine in the Pittsburgh coal seam. In-situ measurements were used to constrain and calibrate the range of DFN parameters in the model. The methodology was then validated against field permeability measurements in a deeper mine, at a 341-m-cover site in the Pittsburgh seam (Khademian et al., 2022). In this paper, another case is studied in a 352-m deep mine, and field permeability measurements are conducted before

and after the first panel mined by the measurement site. The previously developed methodologies were used, and the mining was modeled using a geomechanical model constructed in 3DEC software (Itasca, 2016). The modeling results show the permeability calculated in the model agrees with the field measurements after the first panel mine-by. The measurements will continue until after the second panel mines by the test boreholes in Nov 2023. The modeling results reported here will be compared with the field measurements in a future paper.

DESCRIPTION OF MINE SITE

A longwall mine under 352-m cover in southwestern Pennsylvania in the Pittsburgh coal bed is selected for this study. The Marcellus shale and Pittsburgh coal seam are 1,200–2,100 m apart in the strata but share much of the same areas within Pennsylvania and West Virginia. The selected mine site is located above the Marcellus shale so that to enable shale gas production, gas wells are positioned in longwall pillars used to protect the casing from subsurface deformation. The longwall panel is 456-m wide with a mining height of 2.13 m within a three-entry gateroad system (Figure 1). Overburden geology to the mining depth of 352 m was interpreted by correlating a test site gamma log and a nearby core hole (Van Dyke et al., 2022).

The rock types in the overburden are shale, sandstone, sandy shale, limestone, coal, and shaley limestone with

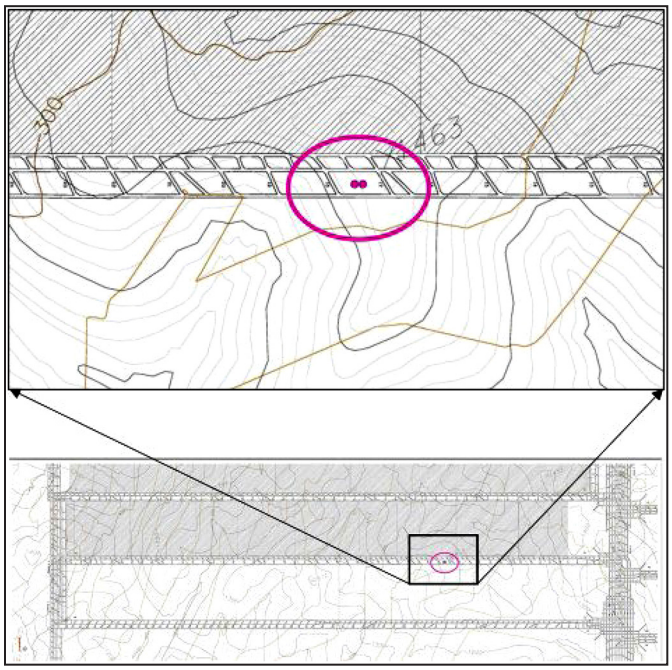

Figure 1. Surface topographical and top-of-coal contours and location of the boreholes for permeability measurements

Table 1. Geomechanical properties applied to the model for each lithology

Rock Type	*E*	ν	*C*	ϕ°	*T*
Coal	2.1	0.3	1.9	28	0.3
Shale	11.6	0.25	11.7	35	4.5
Sandy Shale	11.6	0.25	11.7	35	4.5
Sandstone	11.6	0.22	17.9	35	6.9
Limestone	17.4	0.25	15.9	35	6.1

E: Elastic modulus (GPa), ν: Poisson ratio, C: Cohesion (MPa), ϕ: internal friction angle, T: Tension (MPa)

the field-scale geomechanical properties listed in Table 1 (P. Zhang et al., 2020).

The slug permeability tests are conducted in two boreholes drilled above the abutment pillar (43.7 m width) between the second and third panels in the district. The perforated interval of the first borehole targeted the Uniontown horizon at the depth of 290 m. The second borehole was perforated at the depth of 327 m, targeting the Sewickley horizon. Figure 2 shows the overall overburden geology of the area.

FIELD PERMEABILITY MEASUREMENTS

Two monitoring boreholes were drilled in the overburden to conduct slug permeability tests as the first panel and second panels mine by the test site. Falling-head slug tests were conducted by the research team at regular intervals during the first panel mine-by. The second panel is currently approaching the site, so the data collection is ongoing. The predicted values by the model in this paper will be compared with the measurements once the second panel mines by the test site by November 2023.

Water head pressures were measured at the Uniontown and Sewickley horizons (Figure 2). Permeability values were calculated based on the falling water slug test method detailed in previous works (Harris et al., 2023). An INW PT2X (SeametricsTM) piezometer tracked the long-term equilibrium water height and water slug height.

The data was recorded using the Aqua4TM software package. For the falling-head slug tests, a water slug height of up to 3 m was added to the boreholes. A previous study conducted under shallow cover (127 m to the Sewickley horizon and 76 m to the Uniontown horizon) (Watkins et al., 2021) recorded the fall of water head at 5, 30, or 60-s intervals, depending on the expected drainage rate of the water. Compared to the site described by Watkins et al. (2021), the new site was at a greater overburden depth. Consequently, fracture permeabilities were lower, producing a slower rate of water loss during testing. Therefore,

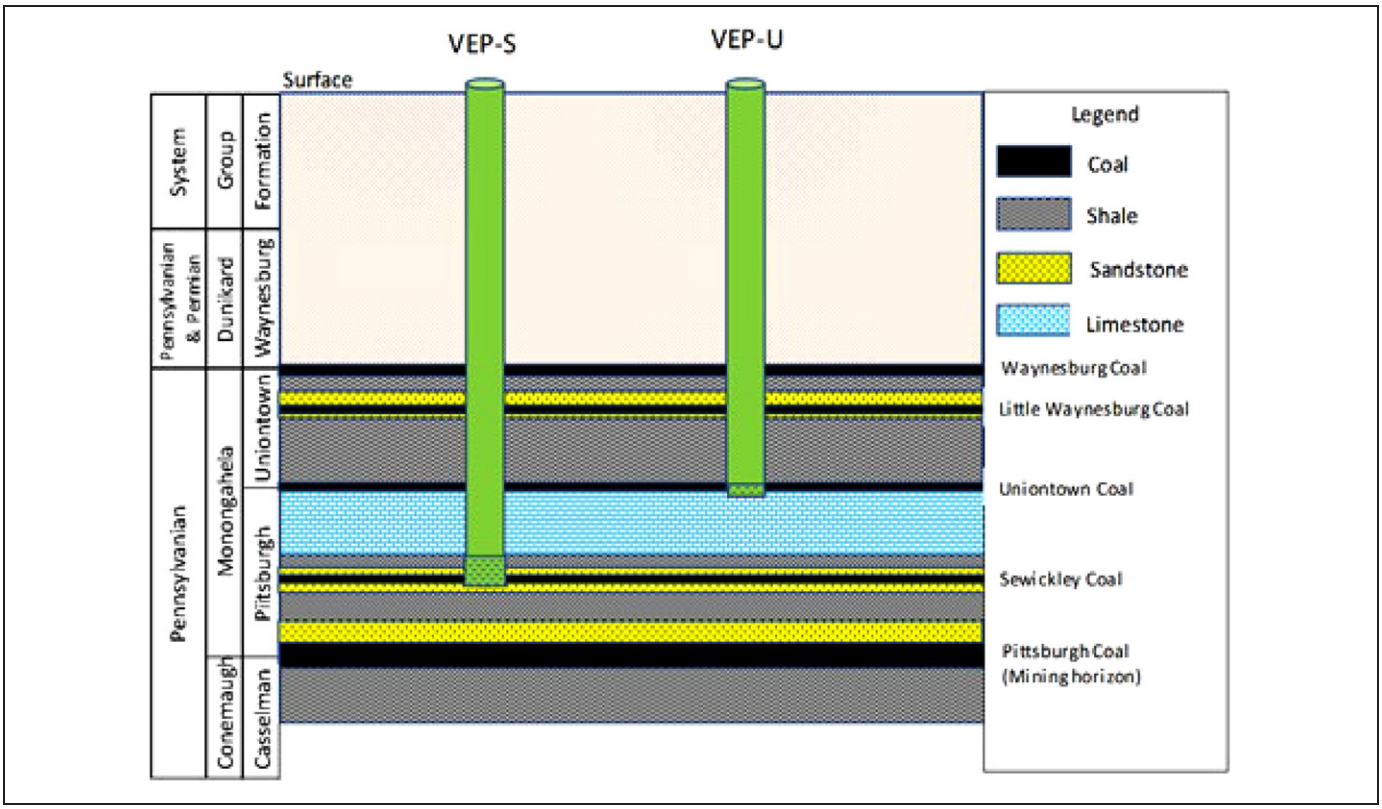

Figure 2. Generalized stratigraphic profile for the monitoring boreholes (not to scale) (Harris et al., 2023)

the data during the longwall mine-by was recorded with a 15-minute interval, and the falling rate was later determined from the downloaded data. Later, after the longwall panel passed the abutment pillar and the permeability values returned to pre-mine-by values, the data was collected every 60 minutes.

The initial H_0 and current H_w water slug heights were recorded by the piezometer and then converted to H_w/H_0 values. H_w/H_0 values were plotted on a semi-log graph to determine the T_{37} time which is the time (minutes) in which the water slug drained to 37% of the initial water slug height. Equation 1 can be used to obtain the absolute permeability of the screened section from T_{37} (Istok, 1992).

$$k = \frac{r^2 \ln\left(\frac{L}{R}\right)\mu}{120\, L\, \rho\, g\, T_{37}} \quad (1)$$

where r is the radius of well casing, L is the length of the well screen, R is the radius of the well screen (the same as well casing in this case), ρ is density of the fluid, μ is the dynamic viscosity of the fluid in kg/ms, and g is the gravitational acceleration. Multiple assumptions are made when calculating permeabilities from slug test head drop or from 3DEC aperture calculations. For the slug test, the permeability is obtained from Hvorsley method with the assumptions that flow in the ground is radially outward and follows Darcy's law. The aquifer is assumed significantly larger than the borehole diameter with an incompressible, homogeneous, and isotropic matrix that is vertically confined by aquicludes.

Figure 3 displays the permeability measurements before, during, and directly after the first panel mine-by.

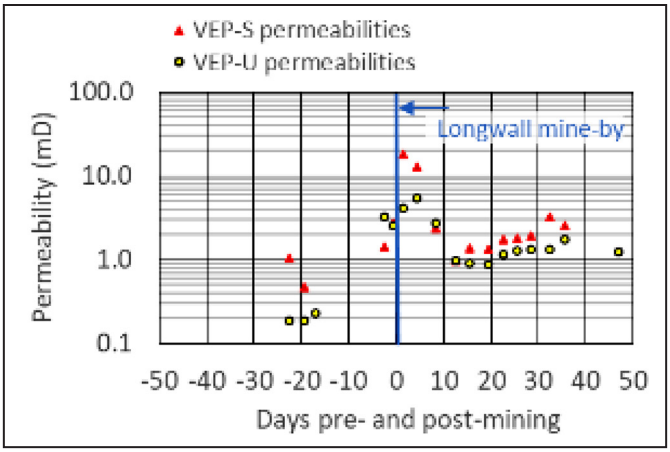

Figure 3. Measured permeability values for the Uniontown (VEP-U) and the Sewickley (VEP-S) horizons under deep cover are shown during the mine-by of the first longwall panel

The first measurements were conducted in August 2021 when the longwall face was 364 m outby the measurement site.

The blue vertical line marks the day of the longwall panel mine-by. At the Sewickley horizon, the highest permeability, 1.76×10^{-14} m^2 (17.8 mD), occurred two days after the first panel mine-by. After the longwall panel mine-by, the permeability values varied in the range of 0.97×10^{-15} m^2 to 1.93×10^{-15} m^2 (0.98 mD to 1.96 mD). For the Uniontown horizon, the maximum permeability under deeper cover was 5.33×10^{-15} m^2 (5.4 mD). After this maximum value, the permeability dropped to a low of 8.78×10^{-16} m^2 (0.89 mD) before slightly rising.

Figure 4 displays the long-term values measured over a period of 22 months. The last measurements were conducted in May 2023 when the face was 1311 m inby. The permeability values +150 days post-mine-by ranged from 0.11×10^{-15} m^2 to 0.29×10^{-15} m^2 (0.11 mD to 0.29 mD) at the Uniontown horizon and 0.09×10^{-15} m^2 to 0.72×10^{-15} m^2 (0.09 mD to 0.73 mD) for the Sewickley horizon.

In summary, the first permeability measurements at the Sewickley and Uniontown horizons were 0.19×10^{-15} m^2 and 1.02×10^{-15} m^2 (0.19 and 1.03 mD), respectively, and are considered to be pre-mine-by permeability values. The last recorded permeability values at the Sewickley and Uniontown horizons were 0.09×10^{-15} m^2 and 0.11×10^{-15} m^2 (0.09 mD and 0.11 mD), respectively, and are considered the post-mine-by permeabilities. The pre- and post-mine-by permeability values were used to validate the geomechanical calculation of permeabilities.

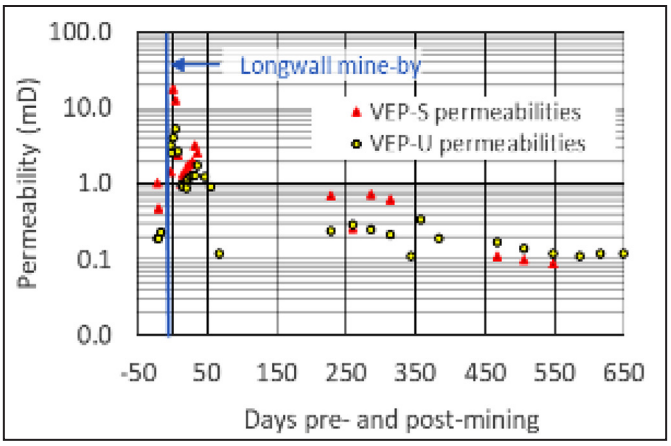

Figure 4. Long-term measured permeability values for the Uniontown (VEP-U) and the Sewickley (VEP-S) horizons under deep cover are shown for the mine-by of the first longwall panel

GEOMECHANICAL MODEL

The 3DEC software is used to construct a pseudo-2D longwall model of the study site (Figure 5) with one-meter length in the out-of-plane direction. DFN is used

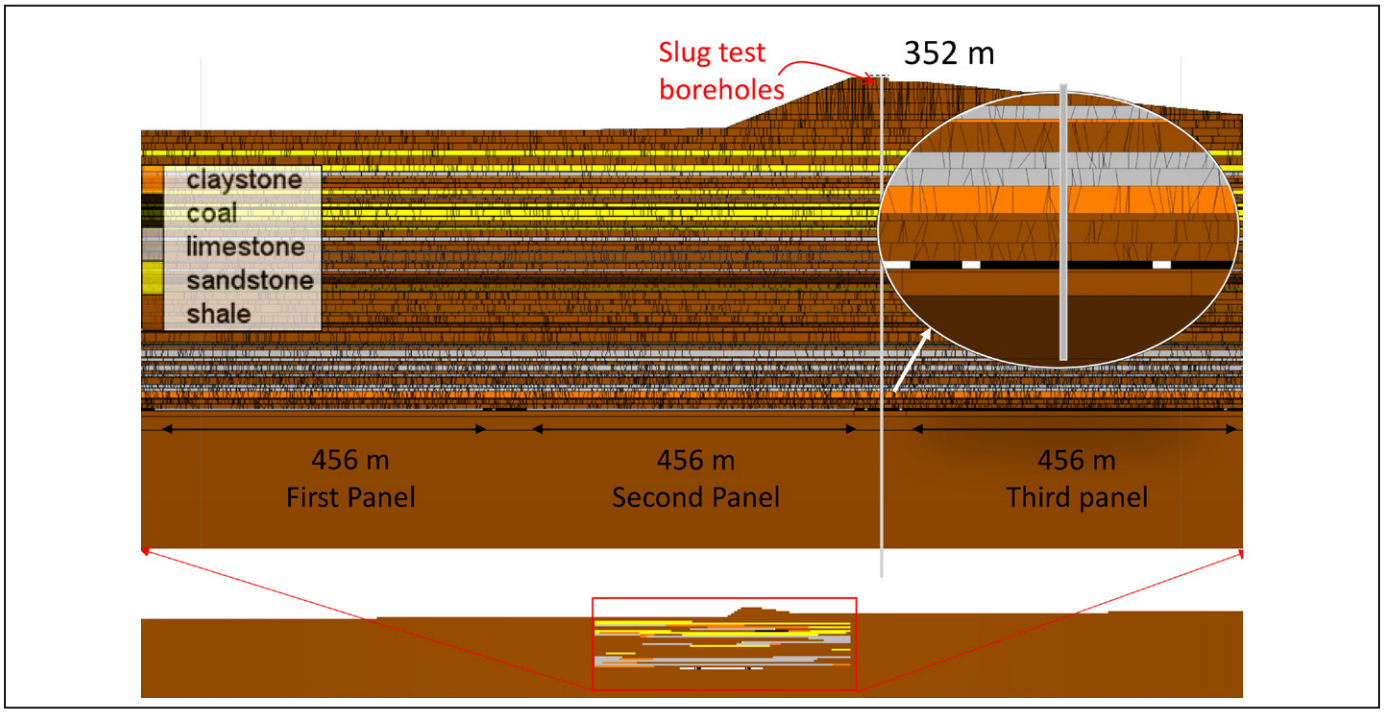

Figure 5. Details of the 3DEC model of the deep longwall mine with DFN elements defining rockmass structures in 105 modeled lithologies

for explicitly modeling fractures in rockmass since the fluid flow through fractures vastly dominates the flow through matrix pores. This is mainly because the cross-sectional area of the fracture, and thus the flow rate through fractures, is several orders of magnitude larger than that of pores within the rock matrix.

Model Geometry

There were 105 geologic layers modeled from the core log data, each with a thickness greater than 0.6 m (Figure 5). The model length is extended in the horizontal direction to a total of 8,000 m to avoid boundary effects on the mining-induced deformations. One of the uncertainties in DFN implementation for fractured rock is in constraining site-specific fracture geometries and frictional properties that best represent rockmass behaviors under stress.

Studying core samples from above abutment pillars in longwall mines suggests propagation of subvertical fractures perpendicular and parallel to the mining face (Van Dyke at al., 2022). Therefore, the DFNs are modeled with a constant dip direction of 90 degrees (perpendicular to the face) and a dip angle with a mean of 90 degrees. From field observations in Southwest Pennsylvania (Kohl, 1980), the variation of the subvertical fracture dip angles is approximated to be 15° from 0–10 m above the mine roof, 12° from 10–30 m, 10° from 30–60 m, and 5° degree for the rest of the domain. Although fracture distribution can be affected by the overall geology of the overburden, depth of mining, panel width, and mining height, the use of values suggested by Kohl (1980) showed promising results for permeability calculations as shown by (Khademian et al., 2021).

The length of fractures is assumed limited to the thickness of host strata with a negative power law distribution and a scaling exponent of 1.1. The position of DFN fractures is defined by a uniform distribution within each individual lithology because pre-mining fracture systems are believed to be the physical properties of the host rock (Feng et al., 2018).

The density of fractures in each stratum is defined as the P_{32} value, which is the cumulated fracture surface per unit volume. Due to the lack of data for the fracture density in this site, the values are based on the previous calibration study on a shallow Pittsburgh coal longwall mine (Khademian et al., 2021). Figure 6 shows the fracture densities in each stratum in the model. Fracture densities range from 0.1 to 0.3 m^2/m^3 with higher values applied to weaker zones that are identified by the logging data and field observations. The weak zones include the shallow weathered zone, Waynesburg horizon, Uniontown horizon, Sewickley horizon, and an interconnected fracture zone mainly caused by the longwall mining. The interconnected fracture zone represents a system of channels allowing flow transport to the mine level. The combined thickness of the caved area and the lower part of the fractured zone above it are known as the interconnected fracture zone.

Through a set of field measurements, Palchik (2003) suggested that the interconnected fracture zone is within 19–43 times the mining height, and Khademian et al. (2021) showed the interconnected fracture zone around

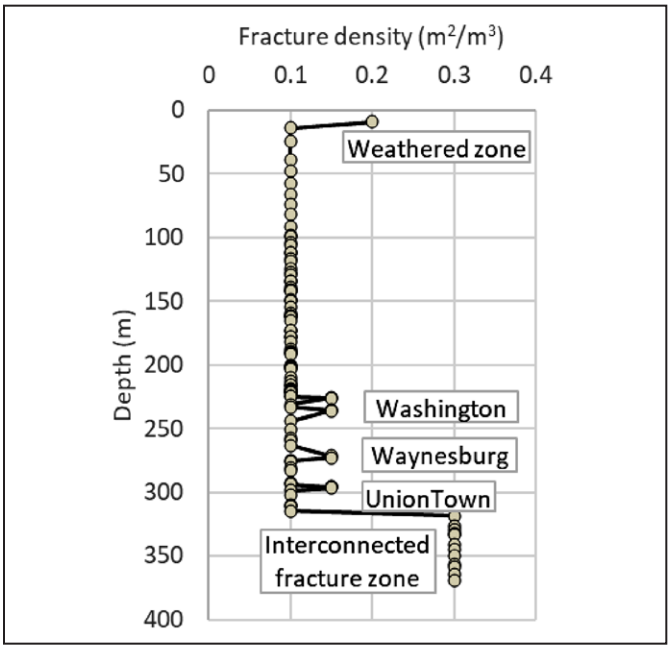

Figure 6. DFN density applied to generate subvertical fractures

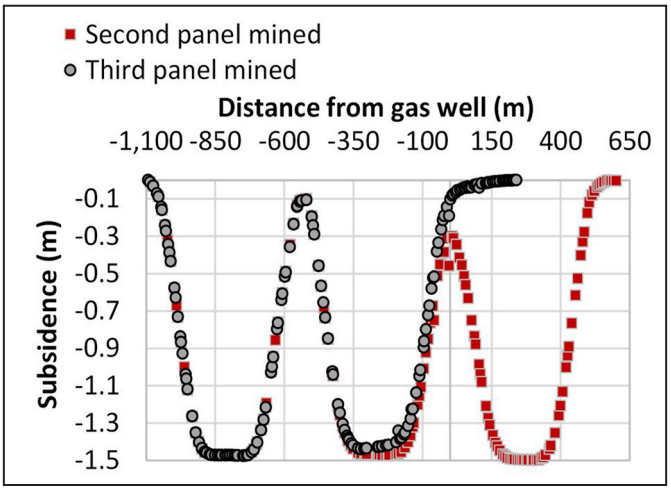

Figure 7. Surface subsidence calculated in the 3DEC model with a maximum subsidence of 1.47 m

23 times offers acceptable results. Thus, the interconnected fracture zone is considered 53-m thick. Following Khademian et al. (2021), the friction of the subvertical DFN fractures and bedding planes are assumed 60% of the internal friction of rock in each stratum, except for the strata within the interconnected fracture zone with a constant friction angle of 10 degrees.

The initial aperture of the fractures in the model needs to be defined before solving the model under in-situ stresses. It is concluded that an initial aperture of 0.4 to 0.5 mm for bedding planes and sub-vertical fractures gives a relatively good agreement between the pre-mining values of permeability from site measurements and models.

Gob Model

In longwall mining, formation of gob material due to the roof caving prevents overstressing the chain pillars. Gob compaction degree and its residual voids affect the overall deformation and stress distribution around the longwall. A gob model in the roof of longwall panels is installed during mining each panel in the model.

Simulation of gob materials in the continuum modeling environment such as FLAC3D can be done with an equivalent element method (Esterhuizen, et al. 2010). In this approach, the caving zone in the model is replaced with zones whose cohesion is reduced during the model run. However, this approach in 3DEC may lead to an excessive overlap of blocks within the equivalent element zones because the DFN-generated blocks can experience large displacement, overlapping the equivalent element zones.

To avoid the excess overlap, Khademian et al. (2022) simulated the effects of the gob materials instead of explicitly modeling the caving process. In this approach, counteracting loads are applied onto the mine roof in the model and are gradually reduced until the mine roof is fully relaxed. At the same time, incremental stresses are applied as gob effects with a=5 MPa and a maximum strain of 44%. Details of the approach can be found elsewhere (Khademian et al., 2022).

Once the model reaches equilibrium, the surface subsidence and pillar stresses are recorded. Figure 7 shows the super-critical surface subsidence recorded in the model with a maximum value of 1.5 m, about 70% of the mining height, that is expected from a supercritical longwall panel. Figure 8(a) and (b) show the modeled pillar vertical stress after the first and second panels are completed, respectively.

In Figure 8, the in-situ vertical stress at the mine level is about 8.9 MPa. The average vertical stress within the abutment pillar (between the second and third panels) increases to 13 MPa and to 24 MPa after the second and third

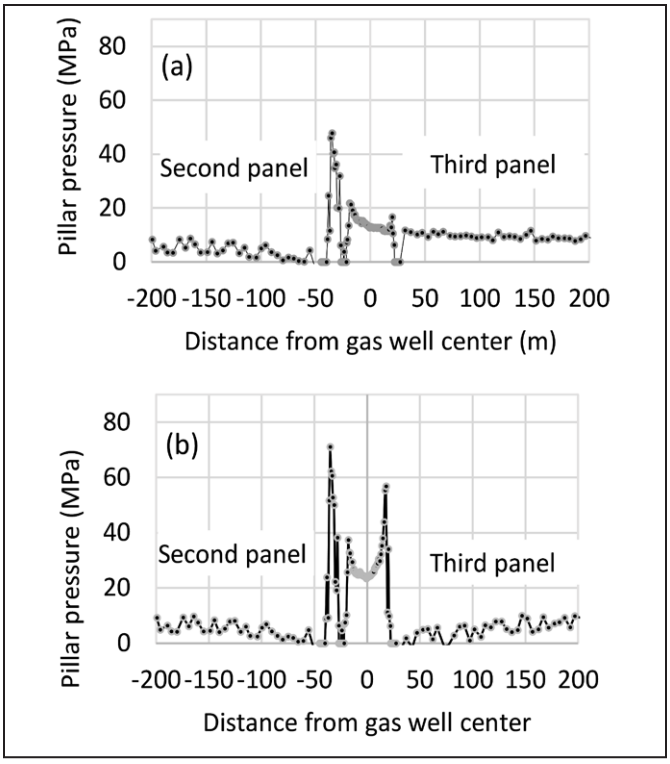

Figure 8. Vertical stress at the mining horizon after mining the second panel (a) and after mining the third panel (b)

panel mining. Figure 8 also shows the gob stress after mining each panel. With the simulated gob effects, the stress within the roof gradually approaches the in-situ stress level of 8.9 MPa, which reflects the expected gob effects after mining the panels.

Aperture Variation

During mining of the two panels, apertures of all fractures are recorded in the model. Figure 9 shows the aperture of the subvertical fractures evolving with the progress of mining in mm. The heat maps are based on a discretization of the 3DEC model with a 17×17 m squares from the roof to the surface of the mine. Values assigned to each square are the average of the aperture of fractures falling within the defined area of the square. The aperture values in Figure 9 correspond to the first, second, and third panel mining. All fractures are initialized with an aperture of 0.3 mm. In-situ stresses expand the range of apertures from 0.3 mm to between 0.005 and 10 mm. This range further expands as mining continues. For visualization purposes the range of the aperture legends are limited between 0.25 mm and 2 mm. The subvertical fractures within the predefined set of DFNs are activated due to the mining-induced deformation and stresses. The activation in shear or tensile modes increases their aperture from the initial values.

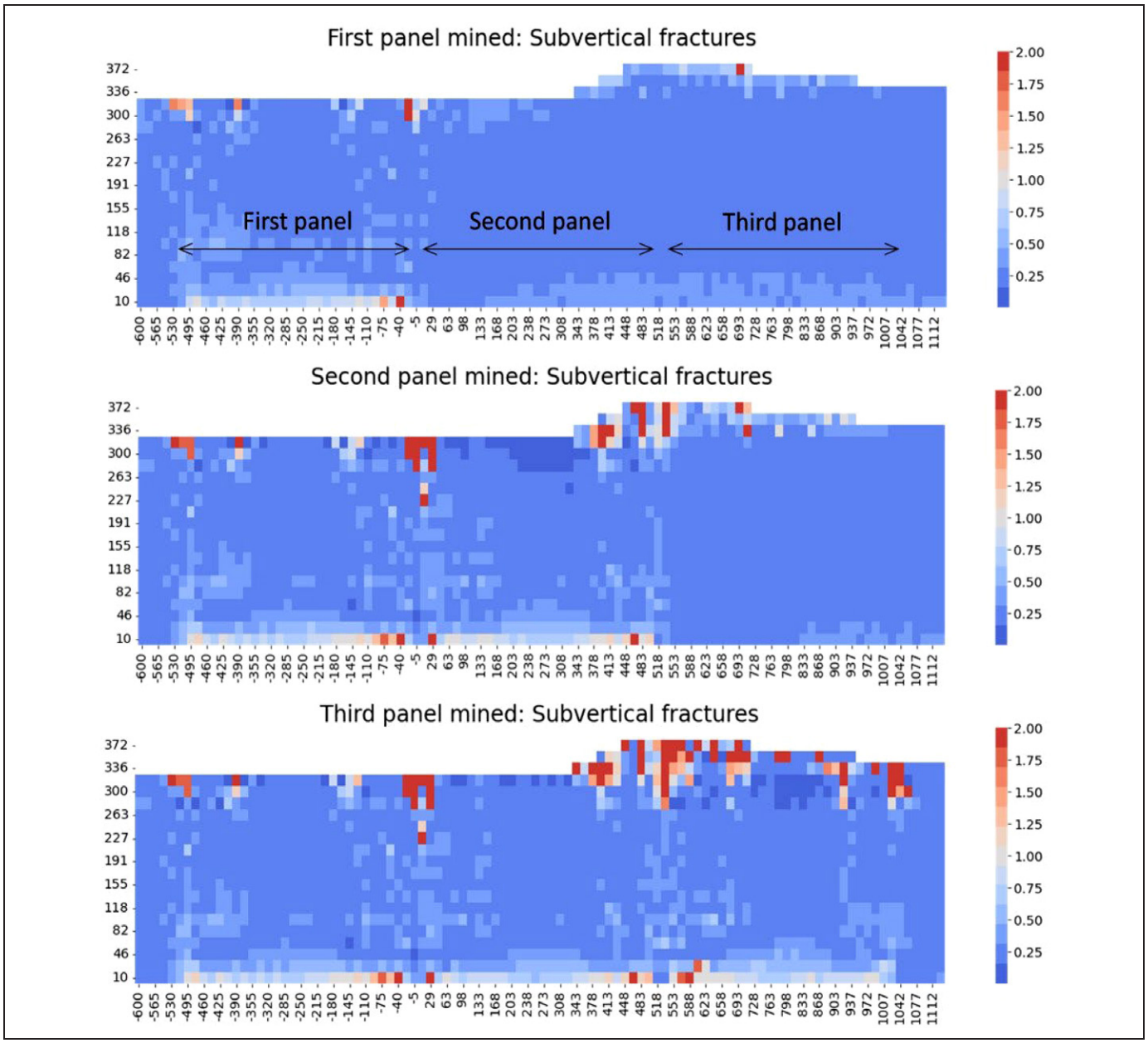

Figure 9. 3DEC results on the aperture values in mm for subvertical fractures (a) after mining the first panel (b) after mining the second panel (c) after mining the third panel

As shown in Figure 9, the fractures located within the caved zone and above the panel edges experience the largest increase in aperture. In contrast, the horizontal stresses induced by mining reduce the aperture of subvertical fractures at the middle of the panels.

Figure 10 shows the aperture plots for bedding plane permeabilities. Bedding plane separation can be seen in the area above each panel but is pronounced above the panel edges and in the caving zone. The lowest aperture values are within the area above the pillars from mine level to 150 m above the roof.

Figure 11 shows the aperture plots for permeabilities of both sub-vertical fractures and bedding planes. The aperture distribution is mainly dictated by bedding planes as they correspond to the larger aperture values. The area with lowest aperture values is still above the pillars but is shrunk to 120 m above the mine.

Permeability Calculation

Rockmass permeability is mostly controlled by the permeability of fractures due to the typically low permeability of the rock matrix. So, it is assumed the rock matrix permeability

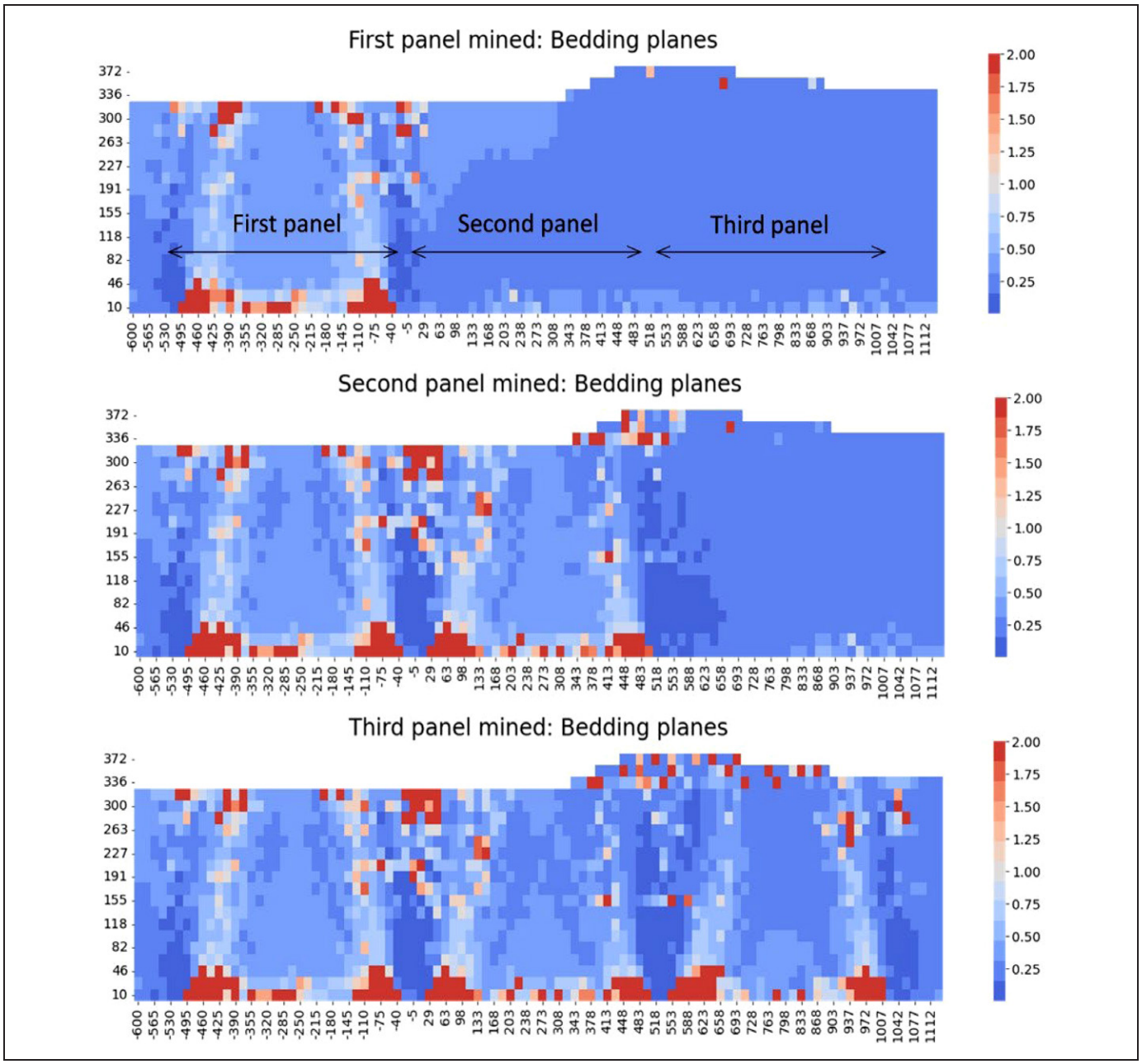

Figure 10. 3DEC results on the aperture values in mm for bedding planes (a) after mining the first panel (b) after mining the second panel (c) after mining the third panel

is zero. The approach for calculating the permeabilities in the model is based on the Cubic Law and Darcy's equation. As part of the calibration efforts, the mechanical apertures are reduced by 60% to represent the hydraulic apertures (Khademian et al., 2021).

The objective here is to calculate permeability values and compare them with the field measurements. The contribution of bedding planes or vertical fractures to the overall of the permeability measured by slug tests cannot quantitatively be determined. Besides, it is not clear what volume of rock surrounding the perforated intervals is represented by the measured permeability of slug tests. However, if the permeability of the borehole wall at the perforation intervals is less than that farther away from the borehole, the lower permeability values determine the flow conditions. Thus, we calculate permeabilities in each layer within a 44-m abutment pillar width and then 22 m radii from the borehole locations and select the minimum values between the two. Based on fracture densities, one may further reduce the length to find the minimum permeability

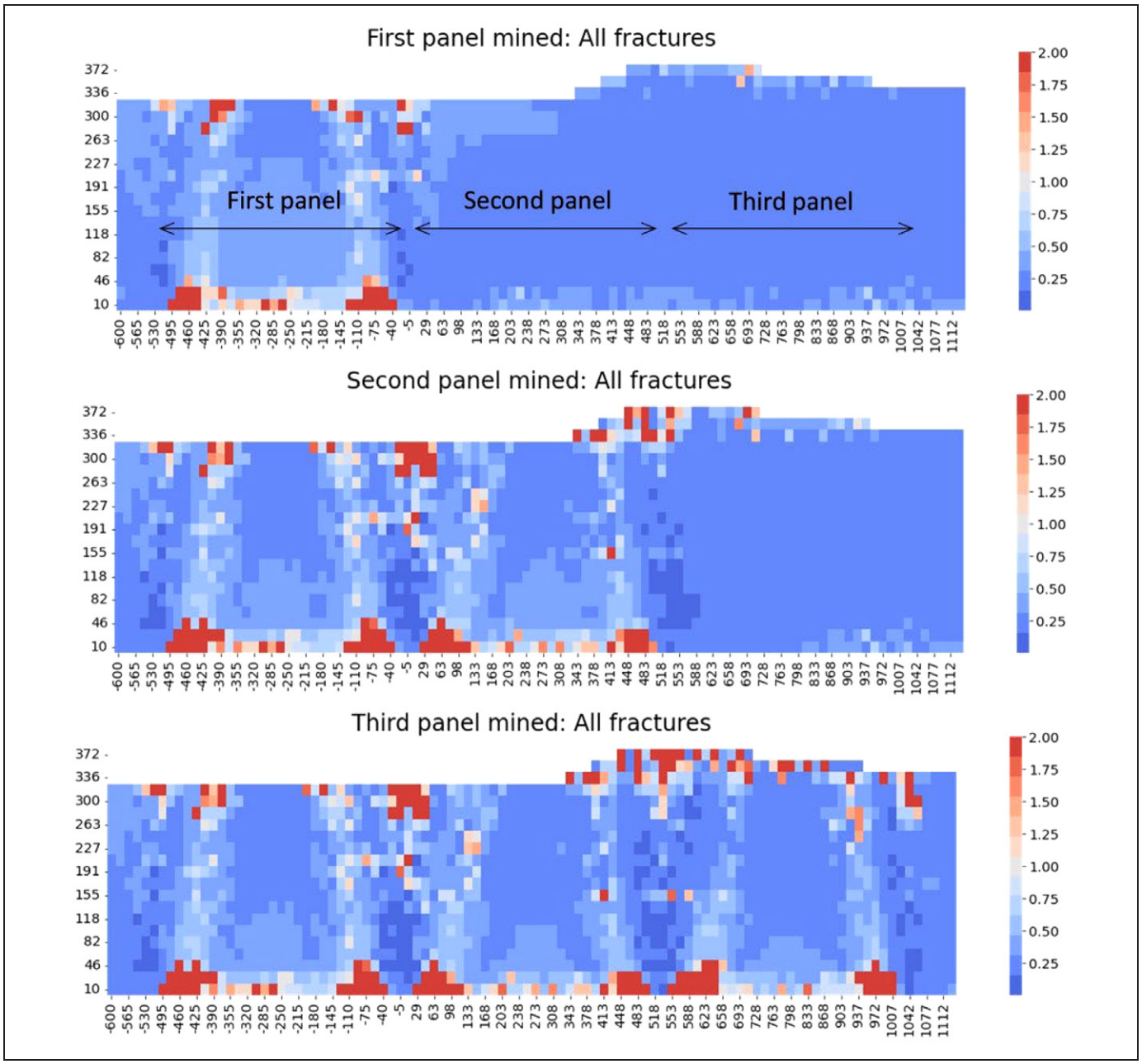

Figure 11. 3DEC results on the aperture values in mm for all fractures (a) after mining the first panel (b) after mining the second panel (c) after mining the third panel

closest to the borehole. The red X's in Figure 12(a) and 12(b) show the field measurement of the permeability values after mining the first and second panels in the model. The modeling results are shown by circles for permeability of sub-vertical fractures and by squares for the permeability of bedding planes. The first and last records of permeabilities in the field are considered as the pre-mine-by and post-mine-by permeabilities, respectively. Figure 12c shows the permeabilities after the third panel is mined. Table 2 lists the predicted values by the model and field measurements.

Field measurements will continue during the third panel mining, and the results will be compared with values in Table 2 in future works. The results listed in Figure 12 and Table 2 show a good agreement between the predicted values in the model and the measured values in the field.

CONCLUSION

A comparison was made between field measurements and the modeled values of rockmass permeabilities above the abutment pillar in a longwall mine in the Pittsburgh coal

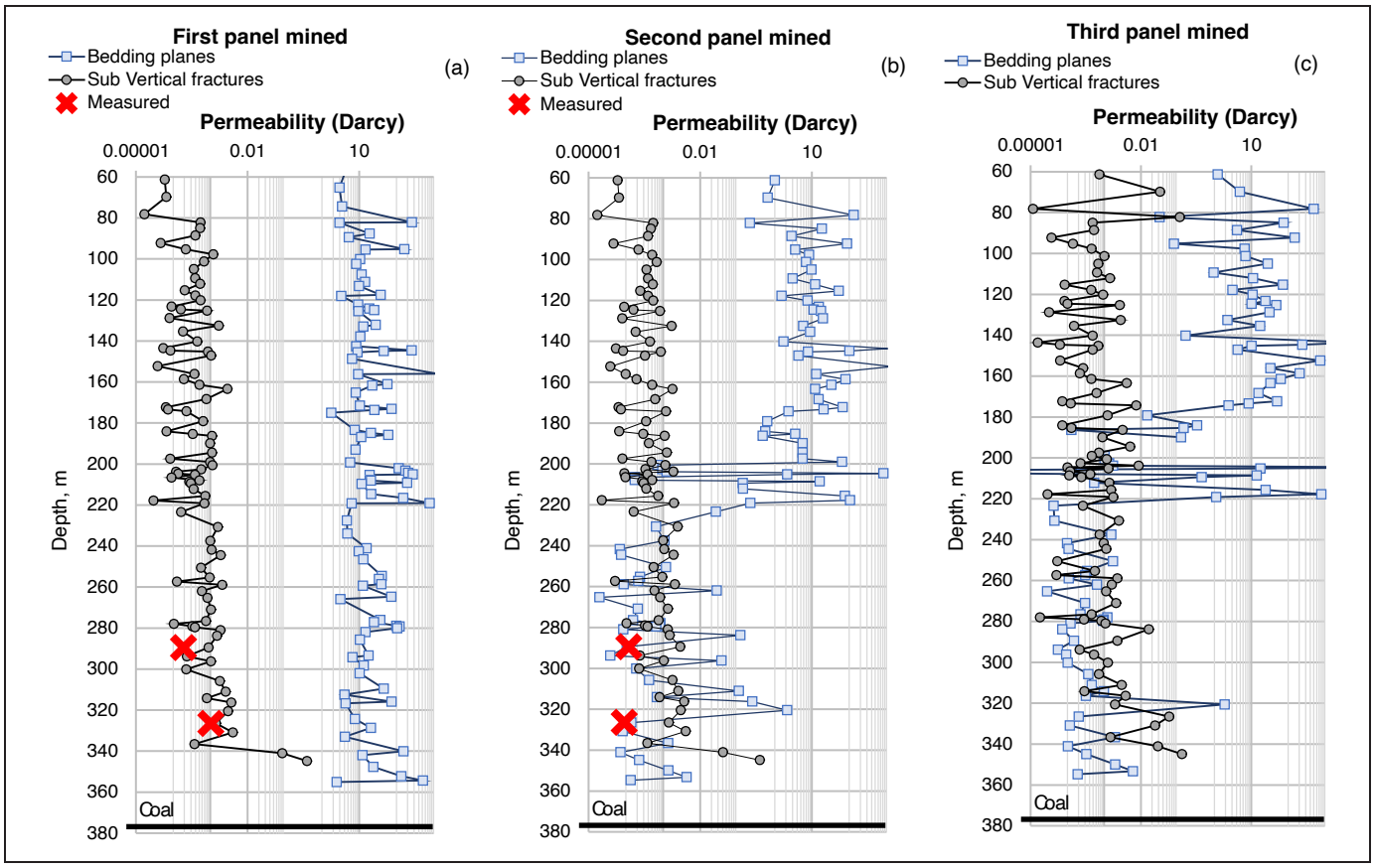

Figure 12. Results of modeled and measured permeability along the depth for (a) first panel is mined, (b) second panel is mined, and (c) third panel is mined

Table 2. Field measurements and model predictions of permeabilities

	Sewickley			Uniontown		
	Model		Field**	Model		Field
	SV	BP	—	SV	BP	—
First panel mined	1.4 mD	20.6 D	1.03 mD	0.9 mD	17.7 D	0.19 mD
Second panel mined	1.4 mD	0.14 mD	0.09 mD	2.9 mD	0.1 mD	0.12 mD
Third panel mined	1.9 mD	0.2 mD	—	2.27 mD	0.15 mD	—

SV: subvertical fractures; BP: Bedding planes; Field: Slug test measurement results

seam under 352-m cover. Two boreholes were drilled above an abutment pillar in the mine. Slug permeability measurement tests were conducted in the boreholes at two perforation intervals located in the Sewickley and Uniontown horizons. A modeling methodology previously developed by researchers at the National Institute for Occupational Safety and Health (NIOSH) was used to investigate the fracture propagation and aperture changes due to mining. It was shown that the minimum aperture values are located in an area above the abutment pillar from the mine roof to 120 m above. The results show that the modeling approach can be used to predict permeability values in similar mining and geologic conditions. Future work can quantify the effects of geological parameters, mining layout, and overburden depth on the fracture aperture evolution and its effects on the rockmass permeability.

LIMITATIONS

This study shows that the field measurement of permeability altered by mining agrees well with the modeling results for a deep cover longwall mine in Southwestern Pennsylvania. However, further work is required to validate the proposed modeling methodology in different geology and operation settings.

DISCLAIMER

The findings and conclusions in this paper are those of the authors and do not necessarily represent the official position of the National Institute for Occupational Safety and Health (NIOSH), Centers for Disease Control and Prevention (CDC). Mention of any company or product does not constitute endorsement by NIOSH.

REFERENCES

[1] Esterhuizen, G. S., C Mark, and M. M. Murphy. 2010. "Numerical Model Calibration for Simulating Coal Pillars, Gob and Overburden Response." 29th International Conference on Ground Control in Mining. Morgantown, WV: Barczak T, ed. 46–57.

[2] Khademian, Z., K. M. Ajayi, D. W. H. Su, G. Esterhuizen, and S. J. Schatzel. 2021. "Geomechanical Modeling of Mining-Induced Permeability: Implications for Potential Gas Inflow from a Sheared Gas Well." 40th International Conference on Ground Control in Mining.

[3] Kohl, W. R. 1980. Jointing in outcropping rocks of Pennsylvanian age, central Greater Pittsburgh region, Pennsylvania. U.S. Geological Survey.

[4] PADEP. 2018. 2018 Oil and Gas Annual Report. Pennsylvania Department of Environmental Protection. Retrieved from 2018 Oil and Gas Annual Report (pa.gov).

[5] Palchik, V. 2003. "Formation of fractured zones in overburden due to longwall mining." Environmental Geology 28–38.

[6] Van Dyke, M., P. Zhang, H. Dougherty, D. W. H. Su, and B. H. Kim. 2022. "Identifying Longwall-Induced Fractures through Core Drilling." Annual Conference of Society of Mining, Minerals, and Exploration.

[7] Zhang, P., D. W. H. Su, H. Dougherty, R. Kimutis, S. Schatzel, and J. Lu. 2020a. "A Case Study on Longwall Mining near Shale Gas Wells in Barrier Pillars—Influence, Safety, and Risks." 54th US Rock Mechanics/Geomechanics Symposium. Golden.

[8] Feng, G., Li, Z., Hu, S., Zhang, Y., Zhang, A., Gao, Q., . . . Cui, J. (2018). Distribution of gob empty space for methane drainage during the longwall mining: A case study. Journal of Natural Gas Science and Engineering, 60, 112–124. doi.org/10.1016/j.jngse.2018.09.026.

[9] Gehne, S., and Benson, P. M. (2019). Permeability enhancement through hydraulic fracturing: laboratory measurements combining a 3D printed jacket and pore fluid over-pressure. Scientific Reports, 9(1), 12573. doi:10.1038/s41598-019-49093-1.

[10] Harris M. L.; Schatzel, S. A., K.; Van Dyke, M.; Zhang, P.; Gangrade, V.; Addis, J. D.; Dougherty, H.; Watkins, E. (2023). Permeability Determination for Potential Interaction between Shale Gas Wells and the Coal Mine Environment due to Longwall-induced Deformations Under Deep Cover. Paper presented at the 19th North American Mine Ventilation Symposium, Rapid City, SD.

[11] Itasca. (2016). 3DEC user manual: Itasca Consulting Group. Retrieved from www.itascacg.com/.

[12] Khademian, Z., Ajayi, K. M., Schatzel, S. J., Esterhuizen, G. S., & Kim, B. H. (2022). Rockmass Permeability Induced by Longwall Mining Under Deep Cover: Potential Gas Inflow from a Sheared Gas Well. Mining, Metallurgy & Exploration, 39(4), 1465–1473. doi:10.1007/s42461-022-00635-8.

[13] Sasaki, T., & Rutqvist, J. (2021). Estimation of stress and stress-induced permeability change in a geological nuclear waste repository in a thermo-hydrologically coupled simulation. Computers and Geotechnics, 129, 103866. doi.org/10.1016/j.compgeo.2020.103866.

[14] Schwartz, F. W., Zhang, H. (2003). Fundamentals of Groundwater. New York: John Wiley & Sons.

[15] Thawatchai, C., Bunpoat, K., and Warakorn, M. (2021). Simulation of rock crack and permeability in dam foundation during hydraulic fracturing. GEOMATE Journal, 21(86), 55–62. Retrieved from geomatejournal.com/geomate/article/view/29.

[16] Tomac, I., and Sauter, M. (2018). A review on challenges in the assessment of geomechanical rock performance for deep geothermal reservoir development. Renewable and Sustainable Energy Reviews, 82, 3972–3980. doi.org/10.1016/j.rser.2017.10.076.

[17] Watkins, E., Karacan, C. Ö., Gangrade, V., and Schatzel, S. (2021). Assessing Gas Leakage Potential into Coal Mines from Shale Gas Well Failures: Inference from Field Determination of Strata Permeability Responses to Longwall-Induced Deformations. Natural Resources Research, 30(3), 2347–2360. doi:10.1007/s11053-021-09859-9.

[18] Zhang, K., Xue, Y., Xu, Z., Su, M., Qiu, D., and Li, Z. (2021). Numerical study of water inflow into tunnels in stratified rock masses with a dual permeability model. Environmental Earth Sciences, 80(7), 260. doi:10.1007/s12665-021-09550-5.

[19] Istok, J. D., and Dawson, K.J. (1992). Aquifer Testing: Design and Analysis of Pumping and Slug Tests (1st edition ed.): CRC Press.

24-094

Wearable Sensors for Continuous, Real-Time Monitoring and Risk Assessment of Mine Workers Health and Safety

Eleonora Widzyk-Capehart
Simtars, Redbank, Queensland, Australia

Gareth Kennedy
Simtars, Redbank, Queensland, Australia

Jupneek Singh
Queensland University of Technology, Brisbane, Queensland, Australia

Leila Safazadeh
VigiLife, Inc., Dayton, Ohio, SA

Jeremy W. Ward
VigiLife, Inc., Dayton, Ohio, USA

Zachary A. Kiehl
VigiLife, Inc., Dayton, Ohio, USA

ABSTRACT

Mine workers are continuously exposed to a host of non-fatal stressors and potentially fatal hazards: noise exposure, excessive vibration, poor air quality, toxicant exposure, ignition of combustible gases, equipment-related accidents, and thermal heat stress.

Wearable or portable sensors and contextual analytics provide a platform to unobtrusively collect and fuse multi-modal health and safety data in real time to compute both acute safety and longitudinal health insights. This paper presents preliminary trial results, conducted by Simtars, VigiLife, Inc., and Queensland Mines Rescue Service, of the application of wearable sensors to monitor heat stress and other vital biometrics for mines rescue personnel.

INTRODUCTION

In the challenging and often perilous environment of mining, the health and safety of mine workers are of paramount concern. Continuous exposure to a myriad of stressors, including overexertion, toxicant exposure, explosions, and thermal heat stress, poses significant risks to their well-being. These risks are exacerbated by the unpredictable mining conditions and varied techniques employed [1, 2]. The consequences of neglecting these risks not only threaten individual miners but also jeopardize the safety and productivity of the mining companies. Among these hazards, heat stress stands out as a particularly insidious threat, as it can lead to fatal outcomes even though it is entirely preventable. In addition, fatigue and chemical exposure are of particular concern in the mining environment. Yet, most organizations in the mining industry lack the technology and tools to predict and mitigate these health and safety risks effectively.

Health Hazards

High-temperature stress conditions can lead to elevated body temperatures among mine workers, thereby increasing the risk of heart-related ailments and potential fatalities [3]. Recent evidence demonstrates a substantial reduction in physical work capacity (i.e., as much as 35–76%) when workers are required to operate in environments with high temperatures and humidity [4]. Research conducted in an underground mine over a 12-month period in Australia reported 106 cases of heat exhaustion requiring medical intervention while similar studies in surface mine operations revealed a high prevalence of heat-related illnesses with 87% of surveyed miners displaying symptoms [5].

Responses to heat stress are governed by a combination of inter-individual factors, such as sex, age, and intra-individual factors encompassing fitness, medication usage, hydration status, shift duration, and illness, as shown in Figure 1.